

Structures and Magnetism of Rubidium and Cesium Salts of Dimeric Oxovanadium(IV) Tarrate(4-) Complexes

JAMES T. WROBLESKI* and MICHAEL R. THOMPSON**

Monsanto Company, Mail Zone Q1B, 800 N. Lindbergh Blvd., St. Louis, Miss. 63167, U.S.A.

(Received March 29, 1988)

Abstract

Complexes of type $A_4[VO(tart)]_2 \cdot nH_2O$, where $A = Rb$ or Cs and tart = *d,l*-tartrate(4-) ($n = 2$) or *d,d*-tartrate(4-) ($n = 2$ for Rb and $n = 3$ for Cs), were prepared from an aqueous mixture of V_2O_5 , AOH and H_4 tart. These complexes were studied by single-crystal X-ray diffraction methods: $Rb_4[VO(d,l-tart)]_2 \cdot 2H_2O$, space group $P\bar{1}$ with $a = 8.156(1)$, $b = 8.246(1)$, $c = 8.719(1)$ Å, $\alpha = 66.09(1)^\circ$, $\beta = 65.07(1)^\circ$, $\gamma = 82.40(1)^\circ$, $Z = 2$, 1917 observed reflections, and final $R_w = 0.035$; $Cs_4[VO(d,l-tart)]_2 \cdot 2H_2O$, space group P_{21}/c with $a = 9.350(1)$, $b = 13.728(2)$, $c = 8.479(1)$ Å, $\beta = 106.77(1)^\circ$, $Z = 4$, 2235 observed reflections, and final $R_w = 0.054$; $Rb_4[VO(d,d-tart)]_2 \cdot 2H_2O$, space group $P_{41}2_2$ with $a = 8.072(1)$, $c = 32.006(3)$ Å, $Z = 8$, 1014 observed reflections, and final $R_w = 0.038$; $Cs_4[VO(d,d-tart)]_2 \cdot 3H_2O$, space group $P_{41}2_2$ with $a = 8.184(1)$, $c = 33.680(5)$ Å, $Z = 8$, 1310 observed reflections, and final $R_w = 0.063$. Bulk magnetic susceptibility data (1.5–300 K) for these compounds and $A_4[VO(l,l-tart)]_2 \cdot nH_2O$ ($A = Rb$, Cs) were obtained on polycrystalline samples. These data were analyzed in terms of a Van Vleck exchange coupled $S = 1/2$ model which was modified to include an interdimer exchange parameter Θ . Analysis of the low-temperature (1.5–20 K) susceptibility data gave $2J = +1.30$ cm $^{-1}$ and $\Theta = -1.86$ K for $Rb_4[VO(d,l-tart)]_2 \cdot 2H_2O$, $2J = +1.16$ cm $^{-1}$ and $\Theta = -1.69$ K for $Cs_4[VO(d,l-tart)]_2 \cdot 2H_2O$, $2J = +1.90$ cm $^{-1}$ and $\Theta = -0.82$ K for $Rb_4[VO(d,d-tart)]_2 \cdot 2H_2O$, $2J = +2.04$ cm $^{-1}$ and $\Theta = -0.80$ K for $Rb_4[VO(l,l-tart)]_2 \cdot 2H_2O$, $2J = +1.52$ cm $^{-1}$ and $\Theta = -0.25$ K for $Cs_4[VO(d,d-tart)]_2 \cdot 3H_2O$, and $2J = +1.64$ cm $^{-1}$ and $\Theta = -0.31$ K for $Cs_4[VO(l,l-tart)]_2 \cdot 3H_2O$. These results suggest the magnitudes of intradimer (ferromagnetic) and interdimer (antiferromagnetic) exchange interactions are similar in these complexes, as observed for the analogous Na salts.

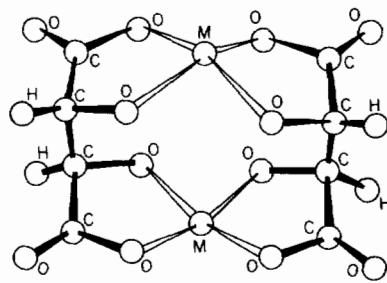


Fig. 1. Generalized structure of dimeric metal($n+$)-tartrate(4-) complexes with bridging tartrate ligands.

Introduction

Structural, electronic, and reactivity properties of tartaric acid [HOOCCH(OH)CH(OH)COOH] isomers, their salts, and metal complexes have been reviewed by Tapscott and coworkers [1, 2]. Tartrate($n-$) complex of general formula $A_{2(n-m)}[M^{m+}(tart^{n-})]_2 \cdot yH_2O$, where tart is *d* (or *l*) or *d,l* (racemic) tartrate($n-$), with the coordination geometry shown in Fig. 1, have been characterized structurally for di[μ -(+)-tartrato(2-)]bis[aquazinc(II)] trihydrate [3], tetrasodium [μ -(+)-tartrato(4-)]- [μ -($-$)-tartrato(4-)]bis[copper(II)] pentahydrate [4], diammonium [μ -(+)-tartrato(4-)] [μ -($-$)-tartrato(4-)]bis[antimony(III)] tetrahydrate [5], tetrasodium [μ -(+)-tartrato(4-)] [μ -($-$)-tartrato(4-)]-bis[oxovanadium(IV)] dodecahydrate [6], tetraammonium di[μ -(+)-tartrato(4-)]bis[oxovanadium(IV)] dihydrate [7], tetrasodium [μ -(+)-dimethyltartrato(4-)] [μ -($-$)-dimethyltartrato(4-)]bis[oxovanadium(IV)] dodecahydrate [8] and hexahydrate [9], as well as others [2].

The dimeric, oxovanadium(IV) tartrate complexes have interesting, and rather unusual, magnetic properties. EPR and magnetic susceptibility studies [10–13] have determined the presence of an intradimer ferromagnetic exchange interaction in these compounds. In the most thorough study of the magnetism of these complexes, Hatfield and coworkers [12] observed that their magnetic susceptibility data were fit to a model which included

*Author to whom correspondence should be addressed.

**Present address: Battelle Pacific Northwest Laboratory, Battelle Blvd., Richland, Wash. 99352, U.S.A.

nearly equal ferromagnetic (intradimer) and anti-ferromagnetic (interdimer) exchange interactions with $J_{\text{inter}} \approx J_{\text{intra}} \approx |1.5 \text{ cm}^{-1}|$.

In order to extend studies of the magnetic properties of the oxovanadium(IV) tartrates, we have prepared and characterized the corresponding Rb and Cs salts from *d,l* and *d,d* tartaric acid. (Preparation of the rubidium salts was described previously [10].) This paper presents results of single-crystal X-ray diffraction and powder magnetic susceptibility studies of these complexes. A preliminary account of this work has appeared [14].

Experimental

The complexes were prepared by the aqueous reaction of high-purity V₂O₅ (Johnson Matthey, PURATRONIC grade, 1 ppm Fe) with excess tartaric acid followed by reaction of the intermediate VO²⁺-tartrate(2-) complex with a stoichiometric amount of alkali metal hydroxide. Thus, for example, V₂O₅ (1.81 g) was added to a solution of *d,l*-tartaric acid (3.30 g) in water (10 ml) and reacted at 70 °C with a subsurface N₂ purge to give a blue product which was treated with 50% aqueous RbOH (8.2 g) to give a red-brown solution. This solution was filtered, reduced in volume at 70 °C, and cooled to room temperature to precipitate well-formed, red-brown crystals of Rb₄[VO(*d,l*-tart)]₂·2H₂O. The *d,d*- and *l,l*-tartrate complexes were violet. See 'Supplementary Material'. Each compound was prepared three times to determine compositional variability. All analyses were consistent with the compositions

A₄[VO(tart)]₂·2H₂O, for A = Rb or Cs, tart = *d,l*-tartrate; A = Rb, tart = *d,d*- or *l,l*-tartrate or A₄[VO(tart)]₂·3H₂O, for A = Cs, tart = *d,d*- or *l,l*-tartrate.

Single-crystal X-ray structure data were obtained at 140 K by using a Syntex/Nicolet P₂₁ autodiffractometer which was equipped with a Nicolet LT1 low temperature device. Suitable single crystals were glued to the end of a 0.10 mm glass fiber. Preliminary lattice constants and probable symmetry and space group were obtained from 25 intense reflections. Intensity data were collected in the θ/2θ scan mode by using graphite monochromated Mo Kα radiation (0.71073 Å). Scans were accumulated 1.0° above and below the calculated K_{α1} and K_{α2} values for each reflection. Background counts were collected at the beginning and end of each scan for a total time interval equal to that used for total peak accumulation time. Reflections were collected in two shells of increasing 2θ: 3.0° to 43.0° at 4.0 deg/min and 43.0° to 55.0° at 3.0 deg/min. Three standard reflections were collected every 100 events as a monitor for crystal deterioration and/or misalignment, neither of which was observed for any compound studied. Standard crystallographic software packages were used for structure refinement. Crystal data and some details of the structure refinement are given in Table I. The structure solution was achieved by Patterson and Fourier methods. All non-hydrogen atoms were refined anisotropically. Hydrogen atoms were located from a difference Fourier map, given isotropic thermal factors, and included in the final least-squares cycles. These final cycles included a least-squares refinable isotropic

TABLE I. Crystallographic Data for Oxovanadium(IV) Tartrates

	Rb- <i>d,l</i> ·2H ₂ O	Cs- <i>d,l</i> ·2H ₂ O	Rb- <i>d,d</i> ·2H ₂ O	Cs- <i>d,d</i> ·3H ₂ O
Formula	Rb ₄ V ₂ C ₈ H ₈ O ₁₆	Cs ₄ V ₂ C ₈ H ₈ O ₁₆	Rb ₄ V ₂ C ₈ H ₈ O ₁₆	Cs ₄ V ₂ C ₈ H ₁₀ O ₁₇
Molecular mass	803.91	992.06	803.91	1011.66
Crystal system	triclinic	monoclinic	tetragonal	tetragonal
Space group	P $\bar{1}$	P ₂ ₁ /c	P ₄ 12 ₂	P ₄ 12 ₂
<i>a</i> (Å)	8.156(1)	9.350(1)	8.072(1)	8.184(1)
<i>b</i> (Å)	8.246(1)	13.728(2)	8.072(–)	8.184(–)
<i>c</i> (Å)	8.719(1)	8.479(1)	32.006(3)	33.680(5)
α (°)	66.09(1)	90.0(–)	90.0(–)	90.0(–)
β (°)	65.07(1)	106.77(1)	90.0(–)	90.0(–)
γ (°)	82.40(1)	90.0(–)	90.0(–)	90.0(–)
<i>V</i> (Å ³)	485.6(2)	1042.1(5)	2085.4(7)	2256.8(9)
<i>Z</i>	2	4	8	8
<i>D</i> _{calc} (g cm ⁻³)	2.749	3.167	3.146	3.026
Size (mm)	0.2 × 0.2 × 0.2	0.2 × 0.2 × 0.2	0.2 × 0.2 × 0.2	0.2 × 0.2 × 0.2
θ limits (°)	3.0–55.0	3.0–55.0	3.0–55.0	3.0–55.0
Unique reflections	2215	2389	1497	1533
Observed reflections	1917	2235	1014	1310
Final <i>R</i>	0.028	0.033	0.038	0.048
Final <i>R</i> _w	0.035	0.054	0.038	0.063
<i>μ</i>	107.02	77.81	100.4	71.996

TABLE II. Atomic Fractional Coordinates for $\text{Rb}_4[\text{VO}(d,l\text{-tart})_2 \cdot 2\text{H}_2\text{O}]^{\text{a}}$

Atom	<i>x</i>	<i>y</i>	<i>z</i>
Rb(1)	0.37727(4)	0.27303(4)	0.33148(4)
Rb(2)	0.83814(4)	0.26277(4)	-0.12957(4)
V	0.24795(7)	0.37106(7)	-0.05354(7)
O(1)	0.4495(3)	0.3260(3)	-0.0601(3)
O(2)	0.2458(3)	0.3784(3)	-0.2835(3)
O(3)	0.2437(3)	0.6234(3)	-0.1731(3)
O(4)	0.1031(3)	0.3829(3)	0.1809(3)
O(5)	0.1065(3)	0.1398(3)	0.0672(3)
O(6)	0.2323(4)	0.5611(3)	-0.5483(3)
O(7)	-0.1047(3)	-0.0377(3)	0.3288(3)
C(1)	0.2358(4)	0.5341(4)	-0.4010(4)
C(2)	0.2187(4)	0.6840(4)	-0.3373(4)
C(3)	-0.0279(4)	0.2459(4)	0.3058(4)
C(4)	-0.0098(4)	0.1015(4)	0.2345(4)
H(1)	0.298(4)	0.776(4)	-0.433(4)
H(2)	-0.014(4)	0.191(4)	0.409(4)
O(w)	0.4211(4)	0.0305(4)	-0.2570(4)
H(w1)	0.456(7)	0.108(7)	-0.234(6)
H(w2)	0.313(9)	0.033(8)	-0.270(8)

^ae.s.d.s given in parentheses.TABLE III. Atomic Fractional Coordinates for $\text{Cs}_4[\text{VO}(d,l\text{-tart})_2 \cdot 2\text{H}_2\text{O}]^{\text{a}}$

Atom	<i>x</i>	<i>y</i>	<i>z</i>
Cs(1)	0.01611(14)	0.13190(2)	0.35269(4)
Cs(2)	0.46197(4)	0.18626(3)	0.32843(4)
V	0.1404(1)	0.39552(7)	0.4422(1)
O(1)	0.2399(5)	0.2978(3)	0.4634(5)
O(2)	0.0065(4)	0.3960(3)	0.2107(5)
O(3)	-0.0443(4)	0.3622(3)	0.4852(5)
O(4)	0.2084(4)	0.4650(3)	0.6451(4)
O(5)	0.2539(4)	0.4995(3)	0.3652(5)
O(6)	-0.2282(5)	0.3733(3)	0.0541(5)
O(7)	0.3862(5)	0.6343(3)	0.4442(6)
C(1)	-0.1345(6)	0.3766(4)	0.1890(7)
C(2)	-0.1733(6)	0.3617(4)	0.3501(7)
C(3)	0.2793(6)	0.5553(4)	0.6361(6)
C(4)	0.3136(6)	0.5666(4)	0.4725(7)
H(1)	-0.220(9)	0.313(5)	0.367(9)
H(2)	0.366(3)	0.562(2)	0.737(3)
O(w)	0.3518(5)	0.4456(4)	0.0863(6)
H(w1)	0.31(1)	0.482(7)	0.03(1)
H(w2)	0.33(1)	0.480(7)	0.20(1)

^ae.s.d.s given in parentheses.

extinction correction and a non-Poisson weight scheme. The *R* values were defined as in eqns. (1) and (2), where *w* is the weight given each reflection, $1/\sigma^2 F_o$.

$$R_1 = \Sigma |F_o| - |F_c| / \Sigma |F_o| \quad (1)$$

$$R_w = [(\Sigma w(|F_o| - |F_c|)^2) / \Sigma w|F_o|^2]^{1/2} \quad (2)$$

TABLE IV. Atomic Fractional Coordinates for $\text{Rb}_4[\text{VO}(d,d\text{-tart})_2 \cdot 2\text{H}_2\text{O}]^{\text{a}}$

Atom	<i>x</i>	<i>y</i>	<i>z</i>
Rb(1)	0.2738(1)	0.2297(1)	0.48741(3)
Rb(2)	0.7707(1)	0.1808(1)	0.19841(3)
V	0.4763(2)	0.0936(2)	0.37818(5)
O(1)	0.6187(1)	-0.0468(7)	0.3794(2)
O(2)	0.5392(7)	0.2272(8)	0.4286(2)
O(3)	0.5267(8)	0.2951(7)	0.3507(2)
O(4)	0.2663(8)	0.0427(7)	0.4028(2)
O(5)	0.3536(7)	0.0235(8)	0.3259(2)
O(6)	0.1098(8)	-0.0607(8)	0.3021(2)
O(7)	0.6286(8)	0.4733(8)	0.4486(2)
C(1)	0.201(1)	-0.016(1)	0.3306(3)
C(2)	0.136(1)	0.000(1)	0.3747(3)
C(3)	0.568(1)	0.434(1)	0.3757(3)
C(4)	0.580(1)	0.380(1)	0.4218(3)
H(1)	0.08(1)	-0.10(1)	0.386(2)
H(2)	0.673(8)	0.485(8)	0.366(2)
O(w1)	0.2371(9)	0.2225(8)	0.0434(2)
O(w2)	0.500	0.086(1)	0.000
O(w3)	0.000	0.484(2)	0.000
H(1w1)	0.2500	0.3242(8)	0.0546(2)
H(2w1)	0.1992(9)	0.1484(7)	0.0546(3)
H(w2)	0.4238(8)	0.1484(9)	0.0175(3)

^ae.s.d.s given in parentheses.TABLE V. Atomic Fractional Coordinates for $\text{Cs}_4[\text{VO}(d,d\text{-tart})_2 \cdot 3\text{H}_2\text{O}]^{\text{a}}$

Atom	<i>x</i>	<i>y</i>	<i>z</i>
Cs(1)	0.7326(1)	-0.2408(2)	-0.01230(2)
Cs(2)	0.2334(1)	-0.1835(1)	-0.30324(3)
V	0.5287(3)	-0.0915(3)	-0.12146(6)
O(1)	0.388(1)	0.047(1)	-0.1190(3)
O(2)	0.468(1)	-0.225(1)	-0.0739(3)
O(3)	0.476(1)	-0.289(1)	-0.1471(2)
O(4)	0.736(1)	-0.042(1)	-0.0982(2)
O(5)	0.647(1)	-0.019(1)	-0.1724(2)
O(6)	0.889(1)	0.057(1)	-0.1947(2)
O(7)	0.390(1)	-0.469(1)	-0.0534(3)
C(1)	0.799(2)	0.016(2)	-0.1676(4)
C(2)	0.864(2)	-0.002(1)	-0.1253(4)
C(3)	0.441(1)	-0.427(2)	-0.1240(4)
C(4)	0.431(2)	-0.375(2)	-0.0803(4)
H(1)	0.90(1)	0.09(1)	-0.127(3)
H(2)	0.34(1)	-0.49(1)	-0.134(2)
O(w1)	0.778(1)	-0.750(2)	-0.7030(3)
O(w2)	0.500	-0.92(2)	-0.500
H(1w1)	0.75(1)	-0.311(9)	-0.447(2)
H(2w1)	0.43(1)	-0.86(1)	-0.979(2)
H(w2)	0.18(1)	-0.68(1)	-0.310(3)

^ae.s.d.s given in parentheses.

The final atomic coordinates are given in Tables II–V. See also ‘Supplementary Material’.

Sites which were occupied by lattice water, O(w), in the *d,l* complexes were occupied fully. Corre-

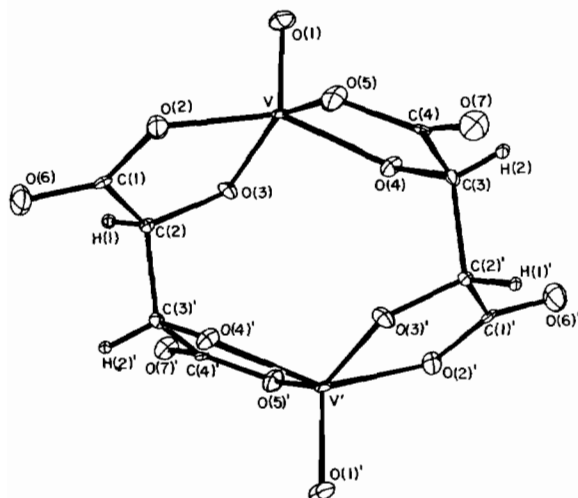


Fig. 2. Structure of the dimeric unit in $\text{Rb}_4[\text{VO}(d,\text{l-tartrate})]_2 \cdot 2\text{H}_2\text{O}$.

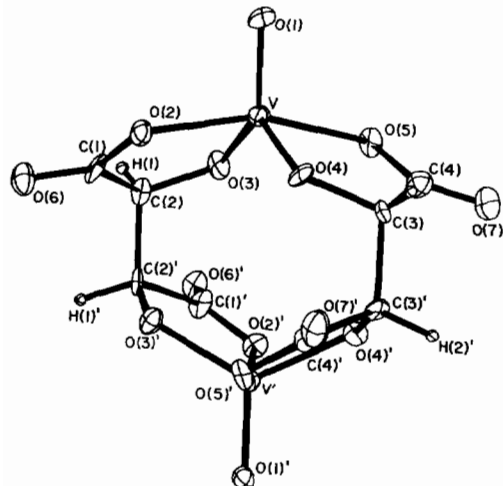


Fig. 3. Structure of the dimeric unit in $\text{Cs}_4[\text{VO}(d,\text{l-tartrate})]_2 \cdot 2\text{H}_2\text{O}$.

sponding lattice water sites for the *d,d* complexes, O(w1), O(w2), and O(w3), were refined as having 0.5 occupancy.

Magnetic susceptibility data were collected from 1.5 to 300 K by using a George Associates force magnetometer system. The magnetic field gradient was measured by using a National Bureau of Standards, cylindrical Pt susceptibility standard. Field intensity was measured with a calibrated Hall probe. GaAs thermometry was used to measure sample temperature. Temperatures below 4.2 K were obtained by pumping on the He bath. Replicate susceptibility measurements of $\text{HgCo}(\text{NCS})_4$ from 4.2 to 300 K were fit to the Curie-Weiss law with $C = 2.358 \pm 0.003$ and $\theta = -1.92 \pm 0.04$ K, in essential agreement with accepted values [15] of 2.351 ± 0.001 and -1.86 ± 0.01 K, respectively. The magnetic susceptibility of $[(\text{CH}_3)_2\text{NHCH}_2\text{CH}_2\text{NH}(\text{CH}_3)_2]\text{CuCl}_4$

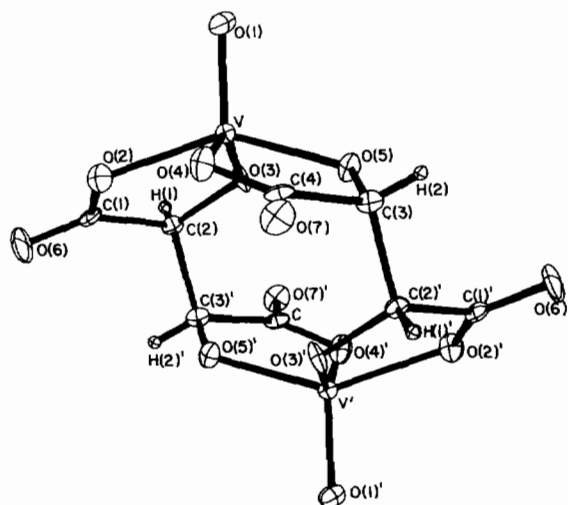


Fig. 4. Structure of the dimeric unit in $\text{Rb}_4[\text{VO}(d,\text{d-tartrate})]_2 \cdot 2\text{H}_2\text{O}$.

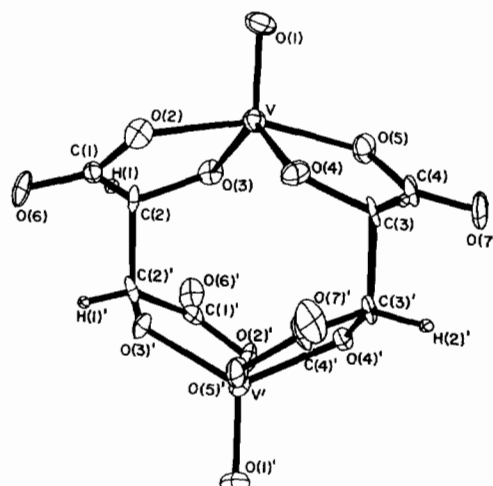


Fig. 5. Structure of the dimeric unit in $\text{Cs}_4[\text{VO}(d,\text{d-tartrate})]_2 \cdot 3\text{H}_2\text{O}$.

was also measured from 4.2 to 50 K to give $C = 0.439$ and $\theta = -0.15$ K, in close agreement with published values [15] of 0.433 and -0.07 K, respectively ($N_\alpha = -217 \times 10^{-6}$ cgsu and $\chi_{\text{dia}} = 60 \times 10^{-6}$ cgsu). Susceptibility data were fit to appropriate theoretical expressions by using a local computer program which incorporated the Simplex minimization algorithm [16]. Diamagnetic corrections were estimated from a table of Pascal's constants [17]. See also 'Supplementary Material'.

Results and Discussion

Structures

The atomic numbering scheme for each compound is shown in Figs. 2 (*Rb-d,l*), 3 (*Cs-d,l*), 4 (*Rb-d,d*), and 5 (*Cs-d,d*). In the *d,l* complexes, primed atoms

TABLE VI. Selected Interatomic Distances (\AA) for $\text{Rb}_4[\text{VO}(d,l\text{-tart})]_2 \cdot 2\text{H}_2\text{O}$ (A) and $\text{Cs}_4[\text{VO}(d,l\text{-tart})]_2 \cdot 2\text{H}_2\text{O}$ (B)^a

	A	B
V–V'	4.231(1)	4.191(2)
V–O(1)	1.619(2)	1.614(3)
V–O(2)	2.002(2)	1.997(3)
V–O(3)	1.918(2)	1.908(3)
V–O(4)	1.916(2)	1.920(3)
V–O(5)	1.989(2)	2.001(3)
C(1)–O(2)	1.291(4)	1.302(5)
C(1)–O(6)	1.235(4)	1.215(5)
C(1)–C(2)	1.518(4)	1.519(5)
C(2)–O(3)	1.394(3)	1.420(4)
C(2)–H(1)	0.87(3)	1.00(7)
C(2)–C(3)'	1.537(4)	1.537(5)
C(4)–O(5)	1.297(4)	1.305(5)
C(4)–O(7)	1.224(4)	1.224(5)
C(4)–C(3)	1.516(4)	1.525(5)
C(3)–O(4)	1.407(4)	1.403(4)
C(3)–H(2)	0.87(3)	0.83(5)
O(w)–H(w1)	0.85(6)	0.73(7)
O(w)–H(w2)	0.93(7)	1.17(7)

^ae.s.d.s given in parentheses.TABLE VII. Selected Interatomic Distances (\AA) for $\text{Rb}_4[\text{VO}(d,d\text{-tart})]_2 \cdot 2\text{H}_2\text{O}$ (A) and $\text{Cs}_4[\text{VO}(d,d\text{-tart})]_2 \cdot 3\text{H}_2\text{O}$ (B)^a

	A	B
V–V'	4.373(1)	4.408(1)
V–O(1)	1.618(6)	1.615(6)
V–O(2)	2.057(6)	2.006(6)
V–O(3)	1.910(6)	1.893(6)
V–O(4)	1.884(6)	1.914(6)
V–O(5)	1.999(6)	2.024(6)
C(1)–O(2)	1.289(11)	1.283(11)
C(1)–O(6)	1.219(10)	1.223(11)
C(1)–C(2)	1.527(12)	1.513(13)
C(2)–O(3)	1.426(10)	1.429(11)
C(2)–H(1)	0.83(8)	0.974(8)
C(2)–C(2)'	1.55(2)	1.55(2)
C(4)–O(5)	1.281(11)	1.297(11)
C(4)–O(7)	1.238(11)	1.206(10)
C(4)–C(3)	1.535(12)	1.543(12)
C(3)–O(4)	1.402(11)	1.416(10)
C(3)–H(2)	1.05(6)	0.984(8)
C(3)–C(3)'	1.53(2)	1.53(2)
O(w1)–H(1w1)	0.76(6)	0.903(6)
O(w1)–H(2w1)	0.79(8)	0.762(6)
O(w2)–H(w2)	1.01(5)	0.976(6)

^ae.s.d.s given in parentheses.

are related to unprimed ones by a pseudo inversion center. In the *d,d* complexes, this relation is by a pseudo two-fold improper axis which bisects the V–V' vector. Selected bond length and angles for the four complexes are given in Tables VI–IX. Rb

TABLE VIII. Selected Intradimer Angles ($^{\circ}$) for $\text{Rb}_4[\text{VO}(d,l\text{-tart})]_2 \cdot 2\text{H}_2\text{O}$ (A) and $\text{Cs}_4[\text{VO}(d,l\text{-tart})]_2 \cdot 2\text{H}_2\text{O}$ (B)^a

	A	B
O(1)–V–V'	156.4(2)	157.4(2)
O(1)–V–O(2)	107.3(1)	106.8(1)
O(1)–V–O(3)	106.5(1)	107.6(1)
O(1)–V–O(4)	107.4(1)	106.5(1)
O(1)–V–O(5)	108.3(1)	106.7(1)
O(2)–V–O(3)	81.7(1)	81.1(1)
O(2)–V–O(4)	145.2(1)	146.5(1)
O(2)–V–O(5)	85.2(1)	85.3(1)
O(3)–V–O(4)	90.6(1)	91.8(1)
O(3)–V–O(5)	145.1(1)	145.5(1)
O(4)–V–O(5)	82.0(1)	82.4(1)
C(2)–C(1)–O(2)	114.5(3)	113.1(3)
C(2)–C(1)–O(6)	121.8(3)	122.7(4)
O(2)–C(1)–O(6)	123.7(3)	124.1(4)
C(1)–C(2)–C(3)'	107.1(2)	107.1(3)
C(1)–C(2)–H(1)	104(2)	122(4)
C(1)–C(2)–O(3)	111.1(3)	111.1(3)
C(3)'–C(2)–H(1)	112(2)	102(4)
C(3)'–C(2)–O(3)	110.5(2)	110.8(3)
H(1)–C(2)–O(3)	112(2)	103(4)
C(2)'–C(3)–C(4)	107.6(2)	107.8(3)
C(2)'–C(3)–H(2)	106(2)	105(1)
C(2)'–C(3)–O(4)	109.7(2)	108.8(3)
C(4)–C(3)–H(2)	108(2)	116(1)
C(4)–C(3)–O(4)	110.6(2)	111.3(3)
H(2)–C(3)–O(4)	114(2)	108(1)
C(3)–C(4)–O(5)	114.3(3)	113.9(3)
C(3)–C(4)–O(7)	121.4(3)	122.3(3)
O(5)–C(4)–O(7)	124.2(3)	123.7(4)
C(1)–O(2)–V	115.9(2)	117.3(2)
C(2)–O(3)–V	116.3(2)	117.0(2)
C(3)–O(4)–V	115.8(2)	115.3(2)
C(4)–O(5)–V	116.2(2)	116.0(2)

^ae.s.d.s given in parentheses.

and lattice water contact distances less than 3 \AA , for the Rb-*d,l* complex are given in Table X.

The coordination geometry about vanadium in the *d,l* complexes is a distorted square pyramid. Distorted trigonal bipyramidal coordination about vanadium in the *d,d* complexes is observed. This coordination environment difference in the two types of complexes results in a significantly longer (*ca.* 0.25 \AA) intradimer vanadium separation in the *d,d* compounds. This coordination difference also increases the O=V–V' angle from about 156° in the *d,l* complexes to about 179° in the *d,d* isomers. These observations are consistent with similar observations made by other workers. Selected intradimer distances and angles for structurally-characterized compounds of this type are given in Table XI. In addition, bond lengths and angles for the tart ligand in the Rb and Cs compounds are similar to those obtained by other workers for coordinated tartrate(4-) anion.

TABLE IX. Selected Intradimer Angles ($^{\circ}$) for $\text{Rb}_4[\text{VO}(d,d\text{-tart})]_2 \cdot 2\text{H}_2\text{O}$ (A) and $\text{Cs}_4[\text{VO}(d,d\text{-tart})]_2 \cdot 3\text{H}_2\text{O}$ (B)^a

	A	B
O(1)–V–V'	178.8(3)	179.1(2)
O(1)–V–O(2)	99.9(3)	100.2(3)
O(1)–V–O(3)	118.0(3)	117.7(3)
O(1)–V–O(4)	117.5(3)	117.3(3)
O(1)–V–O(5)	100.2(3)	99.4(3)
O(2)–V–O(3)	81.2(3)	82.1(2)
O(2)–V–O(4)	87.8(3)	88.5(3)
O(2)–V–O(5)	159.8(3)	160.3(3)
O(3)–V–O(4)	124.5(3)	125.0(3)
O(3)–V–O(5)	90.5(2)	90.5(2)
O(4)–V–O(5)	81.8(3)	80.9(3)
C(2)–C(1)–O(2)	115.0(8)	115.2(8)
C(2)–C(1)–O(6)	120.7(8)	121.1(8)
O(2)–C(1)–O(6)	124.3(9)	123.7(9)
C(1)–C(2)–C(2)'	108(1)	109.0(9)
C(1)–C(2)–H(1)	101.5(6)	101(4)
C(1)–C(2)–O(3)	110.6(7)	111.5(7)
C(2)'–C(2)–H(1)	105.4(6)	113(5)
C(2)'–C(2)–O(3)	110.1(7)	110.4(7)
H(1)–C(2)–O(3)	107.8(9)	122(6)
C(3)'–C(3)–C(4)	105.7(9)	106(1)
C(3)'–C(3)–H(2)	107.6(6)	102(3)
C(3)'–C(3)–O(4)	112.1(7)	113.6(7)
C(4)–C(3)–H(2)	110.4(8)	114(3)
C(4)–C(3)–O(4)	109.4(7)	108.5(7)
H(2)–C(3)–O(4)	111.4(8)	112(3)
C(3)–C(4)–O(5)	114.3(8)	114.6(8)
C(3)–C(4)–O(7)	121.8(8)	122.6(8)
O(5)–C(4)–O(7)	123.9(8)	122.8(8)
C(1)–O(2)–V	116.3(6)	114.6(6)
C(2)–O(3)–V	116.6(5)	116.0(5)
C(3)–O(4)–V	118.0(5)	118.9(5)
C(4)–O(5)–V	116.3(6)	116.5(6)

^ae.s.d.s given in parentheses.TABLE X. Selected Contact Distances (Å) for $\text{Rb}_4[\text{VO}(d,l\text{-tart})]_2 \cdot 2\text{H}_2\text{O}$ ^a

Rb(1)–O(3)	2.887(2)	O(1)–H(w1)	2.76(6)
Rb(1)–O(4)	2.919(2)	O(2)–H(w1)	2.63(5)
Rb(1)–O(6)	2.983(2)	O(2)–H(w2)	2.79(6)
Rb(1)–O(7)	2.901(2)	O(7)–H(w2)	1.96(7)
Rb(2)–O(1)	2.992(2)	O(w)–H(1)	2.71(3)
Rb(2)–O(3)	2.996(2)		
Rb(2)–O(4)	2.927(2)		
Rb(2)–O(6)	2.864(2)		

^ae.s.d.s given in parentheses.

Magnetism

Magnetic susceptibility data, obtained at 6 kOe from ca. 1.5 to 300 K, were obtained for the four complexes which were studied by single-crystal X-ray diffraction. Samples of the corresponding Rb and Cs *l,l*-tartrate complexes were also studied by magnetic susceptibility to check their similarity to the *d,d* isomers.

Powder susceptibility data, from 50 to 300 K, for the Rb complexes, obey the Curie–Weiss law with excellent accuracy. The Cs salts, by contrast, have non-linear inverse susceptibility curves above 150 K. This $1/\chi$ curvature was corrected by adding a temperature-independent term of 35 to 40×10^{-6} cgsu to the data as an empirical correction factor (δ). This factor most likely accounts for an inaccurate estimate for the diamagnetic correction obtained from tables of Pascal's constants [17].

At low temperatures, the observed inverse susceptibility curves for all the complexes show significant deviation from Curie–Weiss law behavior. This deviation is illustrated in the upper plots of Figs. 6–11, which show $\chi_{\text{obs}}^{-1} - \chi_{\text{calc}}^{-1}$ as a func-

TABLE XI. Comparison of Selected Intradimer Distances (Å) and Angles ($^{\circ}$) for VO^{2+} Tartrate Complexes, $\text{A}_4[\text{VO}(\text{tart})]_2 \cdot n\text{H}_2\text{O}$ ^a

A	Tartrate	n	V=O	V–OCO	V–OCH	V–V	O=V–V'	Reference
Na	<i>d,l</i> -tart	12	1.619(2)	2.004(6) 1.994(6)	1.917(6) 1.902(6)	4.082(2)	152.1(2)	6
EA	<i>d,l</i> -tart	8	1.599(3)	2.026(2) 2.021(2)	1.955(3) 1.913(2)	3.985(1)	154.1(1)	18
Rb	<i>d,l</i> -tart	2	1.619(2)	2.002(2) 1.989(2)	1.918(2) 1.916(2)	4.231(1)	156.4(1)	this work
Cs	<i>d,l</i> -tart	2	1.614(3)	2.001(3) 1.997(3)	1.920(3) 1.908(3)	4.191(2)	157.4(2)	this work
AM	<i>d,d</i> -tart	1	1.60(2)	2.03(1) 2.01(1)	1.93(1) 1.79(1)	4.35(1)	177(1)	7
Rb	<i>d,d</i> -tart	2	1.618(6)	2.057(6) 1.999(6)	1.910(6) 1.884(6)	4.373(1)	178.8(2)	this work
Cs	<i>d,d</i> -tart	3	1.615(6)	2.024(6) 2.006(6)	1.914(6) 1.893(6)	4.408(1)	179.1(2)	this work
Na	<i>d,l</i> -mmt	14	1.613(4)	1.991(4) 1.979(3)	1.912(4) 1.904(3)	4.047(3)	155.3(2)	19 <i>(continued)</i>

TABLE XI. (continued)

A	Tartrate	n	V=O	V-OCO	V-OCH	V-V	O=V-V'	Reference
Na	d,l-dmt	6	1.620(3) 1.999(2)	2.030(3) 1.949(3)	1.956(2) 1.949(3)	3.504(1)	153.1(3)	9
Na	d,l-dmt	12	1.623(3) 1.981(3)	2.015(3) 1.964(2)	1.974(2) 1.964(2)	3.429(3)	153.8(2)	8

^ammt = monomethyl tartrate, dmt = dimethyl tartrate, EA = ethylammonium, AM = ammonium; e.s.d.s given in parentheses.

TABLE XII. Magnetic Susceptibility Parameters for A₄[VO(tart)]₂·nH₂O Complexes^a

A	tart	n	Corr × 10 ⁶		EPR \bar{g}	Curie-Weiss law		Modified HDVV dimer (eqn. (3))			Reference
			-X _{dia}	δ		\bar{g}	θ (K)	\bar{g}	2J (cm ⁻¹)	Θ (K)	
Rb	d,l-tart	2	123	0	1.99(2)	1.976(9)	-1.352(8)	1.98(1)	1.30(5)	-1.86(8)	this work
Cs	d,l-tart	2	148	40	1.98(2)	1.981(6)	-1.859(9)	1.96(1)	1.16(6)	-1.69(9)	this work
Rb	d,d-tart	2	123	0	1.99(2)	1.995(9)	-0.437(7)	1.98(1)	1.90(8)	-0.82(8)	this work
Rb	l,l-tart	2	123	0	1.99(2)	1.990(9)	0.000(5)	1.99(1)	2.04(5)	-0.31(7)	this work
Cs	d,d-tart	3	154	35	1.98(2)	1.994(8)	0.087(9)	1.985(9)	1.52(5)	-0.25(9)	this work
Cs	l,l-tart	3	154	40	1.98(2)	1.98(1)	0.266(9)	1.98(1)	1.64(6)	-0.3(1)	this work
Na	d,l-tart	12	165	0	1.972			1.96	4.5	-6.6	13
Na	d,l-tart	12	165	0		1.98	-1.7	1.95	3.0	-1.8	12
Na	d,d-tart	6	125	0		1.96	-0.8	1.93	0.3	-0.3	12
Na	d,l-mmt	10	165	0		1.97	-1.7	1.94	3.4	-1.9	12
Na	d,l-dmt	12	190	0		1.98	-2.1	1.97	4.2	-3.1	12

^ammt = monomethyl tartrate, dmt = dimethyl tartrate; e.s.d.s given in parentheses.

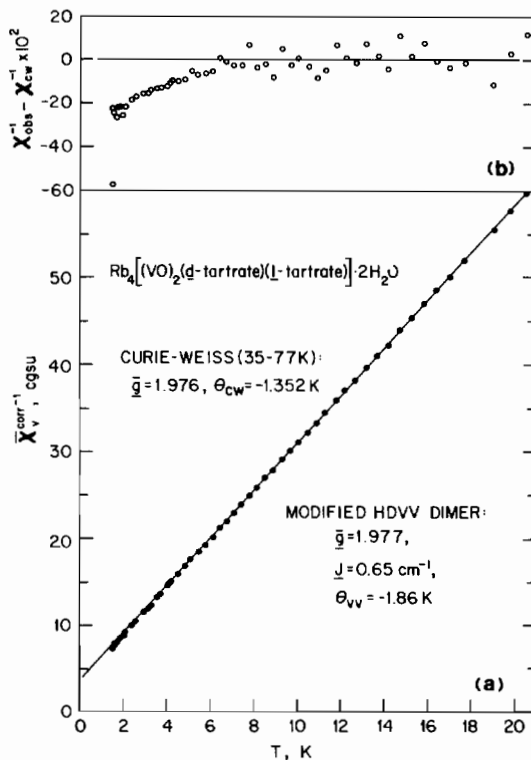


Fig. 6. Low temperature magnetic susceptibility data for Rb₄[VO(d,l-tartrate)₂]·2H₂O: (a) corrected inverse susceptibility vs. T and (b) observed, corrected inverse susceptibility minus calculated Curie-Weiss susceptibility. Best-fit, Curie-Weiss behavior is shown as the solid lines.

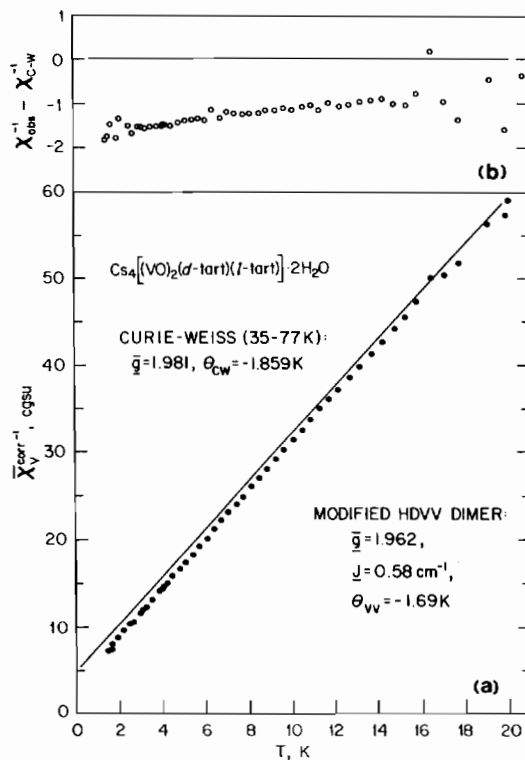


Fig. 7. Low temperature magnetic susceptibility data for Cs₄[VO(d,l-tartrate)₂]·2H₂O: (a) corrected inverse susceptibility vs. T and (b) observed, corrected inverse susceptibility minus calculated Curie-Weiss susceptibility. Best-fit, Curie-Weiss behavior is shown as the solid lines.

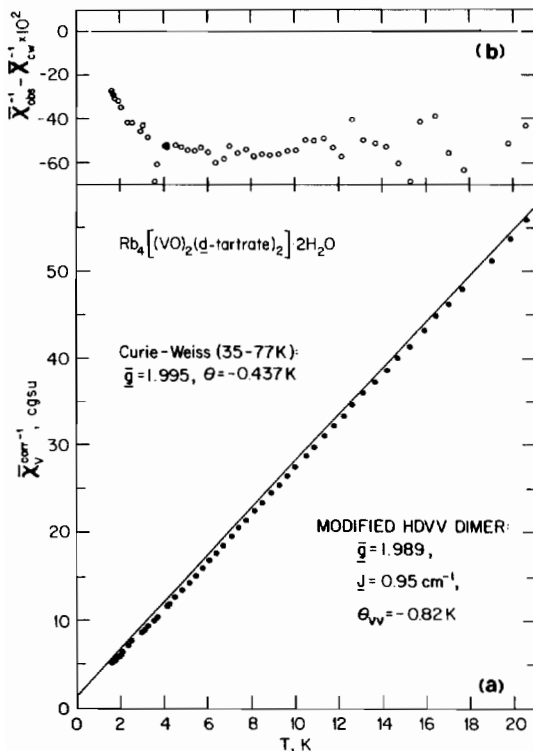


Fig. 8. Low temperature magnetic susceptibility data for $\text{Rb}_4[\text{VO}(d,d\text{-tartrate})_2] \cdot 2\text{H}_2\text{O}$: (a) corrected inverse susceptibility vs. T and (b) observed, corrected inverse susceptibility minus calculated Curie-Weiss susceptibility. Best-fit, Curie-Weiss behavior is shown as the solid lines.

tion of temperature below 20 K. Negative slopes in this residual plot are associated with net antiferromagnetic order whereas positive slopes are associated with net ferromagnetic order. In a modified HDVV model (eqn. (3)), the net antiferro-

$$\chi_m = \frac{N\beta^2 g^2}{3k(T-\Theta)} \left(1 + \frac{1}{3} \exp(-2J/kT) \right) \quad (3)$$

ferromagnetic order results from a lack of balance between $2J$ (which is associated with intradimer spin exchange) and Θ (which is associated with interdimer exchange).

Observed susceptibility data in Figs. 6–11, were described within experimental uncertainty by fitting them to eqn. (3), in which $2J$, g , and Θ were free parameters. Results of the fitting are given in Table XII. Fitted values of g are essentially identical to those obtained from EPR measurements on solid samples of the Rb and Cs salts. As proposed by others [12, 13, 20], observed values of $2J$ are consistent with a ferromagnetic ground state for the dimeric unit in these compounds. Failure to observe the forbidden singlet–triplet transition in the VO^{2+} –tart complexes [20] is consistent with a value of $2J > 1 \text{ cm}^{-1}$. Because Θ and $2J$ have

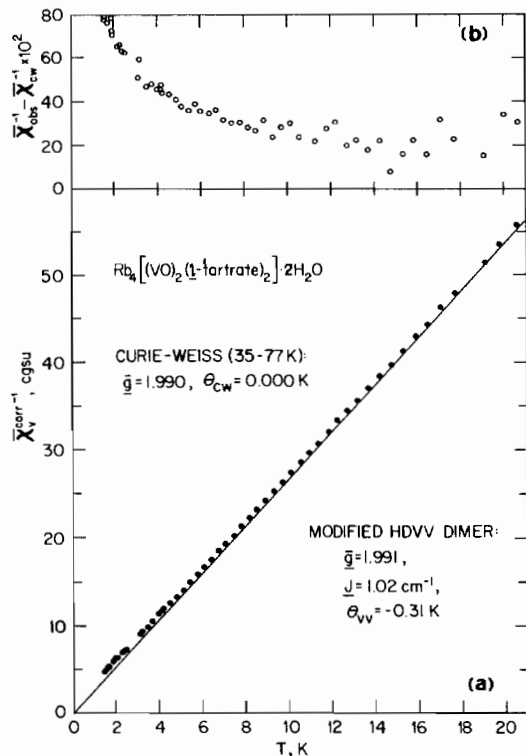


Fig. 9. Low temperature magnetic susceptibility data for $\text{Rb}_4[\text{VO}(l,l\text{-tartrate})_2] \cdot 2\text{H}_2\text{O}$: (a) corrected inverse susceptibility vs. T and (b) observed, corrected inverse susceptibility minus calculated Curie-Weiss susceptibility. Best-fit, Curie-Weiss behavior is shown as the solid lines.

similar magnitudes, it is difficult to speculate further about details of the interdimer exchange mechanism. Indeed, the mechanism of intradimer spin exchange is not completely clear for the tart dimers. Although the zero-field splitting parameter is related to the intradimer V–V separation [20], a direct exchange interaction is improbable based on existing structural and magnetic data for the tart and substituted-tart complexes. Although the effects of sigma-framework tartrate-substitution on the magnetism of these complexes is small, they are not inconsistent with a superexchange mechanism. Perhaps the synthesis and characterization of other substituted tart– VO^{2+} complexes might clarify the exchange mechanism. Single-crystal magnetic susceptibility and EPR measurements on structurally-characterized compounds of this type might also be useful in elucidating the mechanism.

Supplementary Material

Analytical results for the complexes, listings of anisotropic thermal parameters, observed and calculated structure factors, and observed and calculated magnetic susceptibility data, may be obtained from the authors.

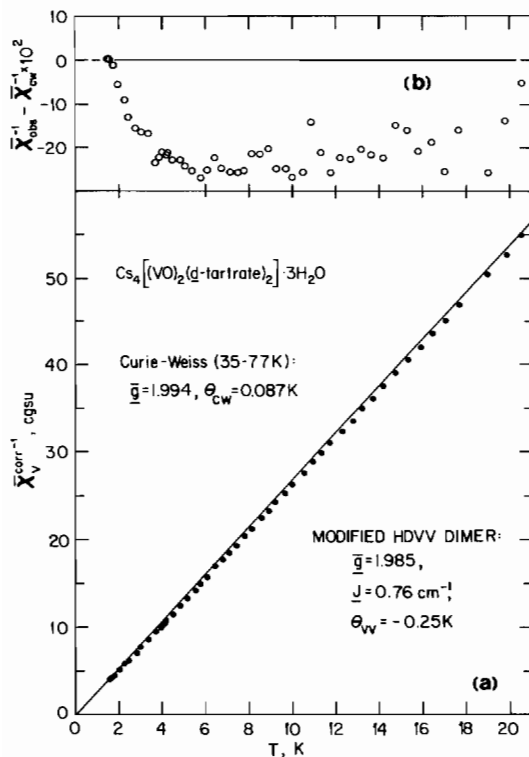


Fig. 10 Low temperature magnetic susceptibility data for $\text{Cs}_4[\text{VO}(\text{d},\text{d-tartrate})_2]_2 \cdot 3\text{H}_2\text{O}$: (a) corrected inverse susceptibility vs. T and (b) observed, corrected inverse susceptibility minus calculated Curie-Weiss susceptibility. Best-fit, Curie-Weiss behavior is shown as the solid lines.

Acknowledgements

The authors thank Catherine Ragland for performing vanadium analyses and Sharon Lemp for obtaining C and H analytical data. We also thank Dr Pierre Berger for obtaining solid- and solution-phase EPR spectra of the complexes reported in this study.

References

- R. E. Tapscott, R. L. Belford and I. C. Paul, *Coord. Chem. Rev.*, **4**, 325 (1969).
- R. E. Tapscott, in G. A. Melson and B. N. Figgis (eds.), 'Transition Metal Chemistry', Vol. 8, Marcel Dekker, 1982, Chap. 3, p. 253.
- L. K. Templeton, D. H. Templeton, D. Zhang and A. Zalkin, *Acta Crystallogr., Sect. C*, **41**, 363 (1985).
- R. J. Missavage, R. L. Belford and I. C. Paul, *Coord. Chem.*, **2**, 145 (1972).
- G. A. Kiosse, N. I. Golovastikov and N. V. Belov, *Sov. Phys. Dokl.*, **9**, 198 (1964).
- R. E. Tapscott, R. L. Belford and I. C. Paul, *Inorg. Chem.*, **7**, 356 (1968).

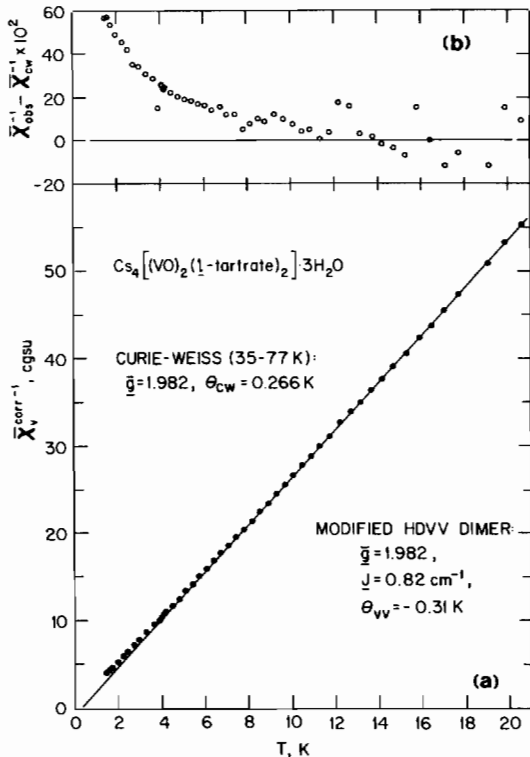


Fig. 11. Low temperature magnetic susceptibility data for $\text{Cs}_4[\text{VO}(\text{l},\text{l-tartrate})_2]_2 \cdot 2\text{H}_2\text{O}$: (a) corrected inverse susceptibility vs. T and (b) observed, corrected inverse susceptibility minus calculated Curie-Weiss susceptibility. Best-fit, Curie-Weiss behavior is shown as the solid lines.

- J. G. Forrest and C. K. Prout, *J. Chem. Soc. A*, 1312 (1967).
- S. K. Hahs, R. B. Ortega, R. E. Tapscott, C. F. Campana and B. Morosin, *Inorg. Chem.*, **21**, 664 (1982).
- H. D. Beeson, R. E. Tapscott and E. N. Duesler, *Inorg. Chim. Acta*, **102**, 5 (1985).
- R. F. Tapscott and R. L. Belford, *Inorg. Chem.*, **6**, 735 (1967).
- M. V. Hanson, C. B. Smith and G. O. Carlisle, *Inorg. Nucl. Chem. Lett.*, **11**, 865 (1975).
- V. H. Crawford, W. E. Hatfield and R. E. Tapscott, *J. Mol. Struct.*, **38**, 141 (1977).
- G. O. Carlisle and G. D. Simpson, *J. Mol. Struct.*, **25**, 219 (1975).
- J. T. Wroblewski and M. R. Thompson, *191st Natl. ACS Meeting*, New York, 1986, Paper No. INOR 367.
- D. B. Brown, V. H. Crawford, J. W. Hall and W. E. Hatfield, *J. Phys. Chem.*, **81**, 1303 (1977).
- S. N. Deming and S. L. Morgan, *Anal. Chem.*, **45**, 278A (1973).
- F. E. Mabbs and D. J. Machin, 'Magnetism and Transition Metal Complexes', Chapman and Hall, London, 1973.
- R. B. Ortega, C. F. Campana and R. E. Tapscott, *Acta Crystallogr., Sect. B*, **36**, 1786 (1980).
- R. B. Ortega, R. E. Tapscott and C. F. Campana, *Inorg. Chem.*, **21**, 672 (1982).
- M. E. McIlwain, R. E. Tapscott and W. F. Coleman, *J. Magn. Reson.*, **26**, 35 (1977).